



HAL
open science

Household aluminum foil matte and bright side reflectivity measurements: Application to a photobioreactor light concentrator design

Victor Pozzobon, Wendie Levasseur, Khanh-Van Do, Bruno Palpant, Patrick Perre

► To cite this version:

Victor Pozzobon, Wendie Levasseur, Khanh-Van Do, Bruno Palpant, Patrick Perre. Household aluminum foil matte and bright side reflectivity measurements: Application to a photobioreactor light concentrator design. *Biotechnology Reports*, 2020, 25, pp.e00399. 10.1016/j.btre.2019.e00399. hal-02949108

HAL Id: hal-02949108

<https://hal.science/hal-02949108>

Submitted on 21 Dec 2021

HAL is a multi-disciplinary open access archive for the deposit and dissemination of scientific research documents, whether they are published or not. The documents may come from teaching and research institutions in France or abroad, or from public or private research centers.

L'archive ouverte pluridisciplinaire **HAL**, est destinée au dépôt et à la diffusion de documents scientifiques de niveau recherche, publiés ou non, émanant des établissements d'enseignement et de recherche français ou étrangers, des laboratoires publics ou privés.



Distributed under a Creative Commons Attribution - NonCommercial 4.0 International License

Household aluminum foil matte and bright side reflectivity measurements: application to a photobioreactor light concentrator design

Victor Pozzobon^{a,*}, Wendie Levasseur^a, Khanh-Van Do^b, Bruno Palpant^b, Patrick Perré^{a,c}

^aLGPM, CentraleSupélec, Université Paris-Saclay, SFR Condorcet FR CNRS 3417, Centre Européen de Biotechnologie et de Bioéconomie (CEBB), 3 rue des Rouges Terres 51110 Pomacle, France

^bLPQM, CentraleSupélec, Université Paris-Saclay, 3 Rue Joliot Curie, 91190 Gif-sur-Yvette, France

^cLGPM, CentraleSupélec, Université Paris-Saclay, 3 Rue Joliot Curie, 91190 Gif-sur-Yvette, France

Abstract

This work reports the design of a light concentrator intended to be used to cast uniform lighting over a photobioreactor. Household aluminum foils was chosen as reflective material to build the concentrator. This choice raised the question of which side to use. Thus measurements of household aluminum foil reflectivity spectra on both bright and matte sides were undergone. These measurements were done using an integrating sphere, over a 250 - 2500 nm range. Diffuse and total reflectivities were acquired, for two samples each time. The obtained results are very repeatable and in good agreement with literature on rolled aluminum sheets, for the bright side at least, as matte side data were not found. Specular reflectivity is higher for the bright side while diffuse reflectivity is higher for the matte one. Furthermore, both sides of the foil have the same total reflectivity, around 86 % in the visible range of the spectrum, 97 % in the near infrared. Our measurements are readability usable and available as supplementary materials. Finally, we applied these findings to the in silico design of lab scale light concentrator illuminating a new photobioreactor. A modified version of the raytracing software Soltrace was used to determine which of the two sides of our household aluminum foil was be best suited for our application.

Keywords: Aluminum foil, Reflectivity, Specular, Diffuse, Light concentrator, Photobioreactor

1. Introduction

Household aluminum foil has a wide range of applications in engineers and researchers day to day lives, from a means of protecting the food for lunch, to an handy way to shade photosensible samples from light. Indeed, these foils are mechanically robust, water-proof, light weight, long lasting and affordable.

5 Our interest in this material emerged from our project to develop a new photobioreactor to study the impact of lighting conditions on microalgae growth. To do so, we designed a flat panel photobioreactor (1; 2; 3) with the aim of providing an homogeneous light field to the culture. In order to achieve such conditions, the reactor has to be very thin (width×length×thickness 5×12×0.6 cm³) and the incident light field should be uniform. The light source should also be flexible in terms of power and light / dark cycles. Hence, we choose a dimmable LEDs panel as light
10 source.

There are two ways of obtaining an uniform light field on the surface of the reactor:

- place the LEDs panel in contact with the reactor. It would be very simple and yield a high luminous flux on the reactor surface. Sadly, it would lead to an overheating of the photobioreactor and the loss of the culture

*Corresponding author

Email address: victor.pozzobon@centralesupelec.fr (Victor Pozzobon)

- place the LEDs panel further away from the reactor and use a light concentrator.

15 The second option was chosen. The foreseen design is pictured in Figure 8. The LEDs panel would be placed at one end of a rectangular shaped concentrator, while the photobioreactor would be at the other end. The inner faces of the concentrator would be coated with aluminum foil as it is unexpensive and highly reflective. Yet this choice raised the question of which side of the foil would be best suited. To address this question, we first started by an extensive literature survey. Among the studies openly reporting the use of household aluminum foil, mostly
20 as light reflector, one can note its employment to:

- increase photosynthetically active radiation on growing plants (4), improving the production of fruits per plant by 48 %, seeds weight by 57 %, total biomass by 50 %,
- enhance bacteria removal in low-tech, low-cost, water purifier (5), lowering the disinfection time by 46 %,
- to inexpensively reflect more solar radiation onto a photovoltaic module (6)(7), boosting its production by 14
25 %, build a concentrated solar power thermal system (8) or a solar cooker (9)
- to protect heat sensor from unwanted radiation (10).

Yet their use remains under reported in the literature.

From a manufacturing perspective, aluminum foils are defined as aluminum sheets with a thickness below 200 μm . Usually household foils is 16 μm thick, up to 24 μm for heavy duty. Industrially such low thicknesses are
30 achieved by successively rolling foils between twin rolls mills (11). During the latest rolling stages, in order to prevent the foils from shredding, two foils are rolled together. As a result household aluminum has two sides: a bright mirror-like one (in contact with the rolls) and a matte one (in contact with the other foil).

Sadly after this survey, we found that no scientific article dealing with this question. Only that out of common knowledge (12), it is admitted that both sides would have the same reflectivity, even though an obvious difference
35 exists. Furthermore, the few authors admitting using aluminum foil did not precise which side of the foil was used. Had they done it, it could have been used as guideline. The lack of published articles dealing with household aluminum foils reflectivity does not mean that aluminum was not studied as a reflecting material. On the contrary, given its high reflectivity and low absorptivity (13), it is commonly used to produce mirrors. Two production techniques exist:

- Physical Vapor Deposition (PVD) is the technique yielding the best reflectivity, usually higher than 90 %
40 (14)(15)(16). It consists in vaporizing aluminum under a low pressure atmosphere before depositing it as a thin film on an optically polished surface. As it is an expensive technique, it is reserved to high end applications such as: internal mirrors for spectrophotometers, lasers, astronomers instruments (15)(14)(17)(18)(19), radiative heat shields for space applications (16), rust-proof coating (20)(13) and, of course, high quality solar mirrors
45 (21).

• Rolling consists in thinning of an aluminum sheet between twin rolls right after the casting stage. This process can produce mirror-like surfaces at a much lower cost than PVD. Its products are usually used when one has to keep costs in mind and mechanical robustness is sought after. To this regard, aluminum has been shown to be 5.6 to 81 % more efficient than stainless steel, depending on the application (6)(8). Numerous authors have used and investigated the capabilities of rolled aluminum sheets in the context of solar energy recovery (22)(23)(8)(23)(24), or in a more general manufacturing context, such as car shininess (25)(13), wastewater treatment (26) or even goat milk pasteurization (27). Furthermore the rolls passings are known to leave stripes on the aluminum foil (11). These stripes tend to orient reflected light and make light reflection non-isotropic (23)(28)(29). More generally, aluminum sheets reflectivity is affected by the alloy purity (30) and surface roughness. As a good rule of thumb, the higher the roughness - or number of roll passings - the lower the total reflectivity and the higher the diffuse component of this reflectivity (21)(29)(31). Nevertheless, if need be, aluminum sheets reflectivity can be improved by chemical etching or electrochemical polishing (25)(14).

All those studies give valid points of comparison for new results. Furthermore, mirrors manufacturers data should not be disregarded. They have been reviewed by Harisson (16).

In the absence of literature dealing with the optical properties of household aluminum foils, we decided to undertake optical characterization of this material. To do so, both bright and matte sides of a commercially available aluminum foil were analyzed using an integrating sphere, yielding specular, diffuse and total reflectivity of the material. Those measurements are reported in this article and available as additional materials. Going one step further, Soltrace (32), an open source raytracing software was used to, in silico, design our lab scale light concentrator and decide which side of the foil would we use.

2. Materials and methods

2.1. Aluminum foil sample

Two 2×2 cm² samples were cut from a roll coming from a general public supermarket. The foil thickness was measured to be 12.5 ± 2.5 μ m. SEM observations were carried out to qualitatively analyze the foil surfaces (Fig. 1). On one hand, the bright side exhibits parallel, evenly spread, stripes. On the other hand, the matte side does not show such stripe but is somewhat more hilly. These observations are in agreement literature, the stripes being the marks left by the twin roll mills. Furthermore, some small debris, appearing in white in the pictures, can be found on the surface. They are aluminum fines that are trapped and latter deposited by the mills (11).

There was no reference regarding the aluminum alloy used to produce this foil. Hence, energy-dispersive X-ray spectroscopy was used to determine the foil composition. The associated spectrum is reported in Figure 2. From this measurement, the alloy composition was determined, with an uncertainty of ± 1 %. The main component is

aluminum (93.84 %) followed by oxygen (4.14 %), calcium (1.20 %) and iron (0.82 %). While calcium presence cannot be explained, iron gives a serious hint toward a Al 8xxx alloy. These series of alloy are usually associated with higher strength, better formability, and improved stiffness, which is coherent with its use to produce foils. Oxygen presence can be explained by the fact that during the foil production stage, a thin layer of aluminum oxide is formed within the first minutes of contact with oxygen (15). This layer thickness depends on contact duration, atmosphere pressure and composition. It ranges from 1 or 2 nm, for low pressure deposition techniques (17), up to 9 nm, for aluminum left exposed to the atmosphere for days until the oxide layer growth becomes diffusion limited (13)(25). In our case, it is safe to assume that the samples were coated with a layer of about 9 nm of aluminum oxide.

In order to characterize the samples further, roughness measurements were carried out using STIL Microtopograph CHR 150-N (z precision 10 nm). Figure 3 reports both bright and matte sides roughness maps (scene 50x50 μm^2 , spatial resolution 0.2 μm). Bright side measurements confirm the presence of parallel stripes, while the matte side features randomly uphill and downhill alternation. Furthermore, the bright side exhibits a lower roughness ($R_a = 0.200 \pm 0.01 \mu\text{m}$) than the matte one ($R_a = 0.459 \pm 0.06 \mu\text{m}$).

Finally, during our anyalysis, the samples were manipulated with gloves, degreased on both sides using ethanol and stored in an air-tight container to prevent dust deposit or accidental deterioration (14)(23).

2.2. Reflectivity measurements

The specular and total reflectivity measurements were done using a Cary 5000 (Agilent, deuterium arc lamp for UV, quartz tungsten-halogen lamp for VIS-IR, with PMT detector for UV-VIS and cooled PbS for NIR) spectrophotometer mounted the DRA2500 integrating sphere (diameter 110 mm, coating Spectralon SRS-99). They cover a range from 250 to 2500 nm. This measurement method was already sucessfully used by several other authors (21)(23)(22)(29)(33).

Figure 4 (a) presents the sphere mounting allowing for diffuse reflectivity measurement. The sample is exposed, through an aperture in the sphere, to a normal incident beam. The specular component of the reflection is sent back through the aperture while the diffuse component is successively reflected until it reaches the detectors. In our case, we used a reduced aperture with a surface of $9.08 \times 5.10 \text{ mm}^2$, corresponding to $\pm 2.4^\circ$ azimuth and $\pm 1.3^\circ$ elevation, or about 0.004 sr. Specular, or more precisely near specular, reflection is commonly considered to be comprised within 0.01 sr (23).

Total reflectivity measurement is pictured on Figure 5 (b). In this configuration, the sample is tilted with a $3^\circ 20'$ min angle so that the specular component of the sample reflection is directed toward the sphere internal coating. Hence, both specular and diffuse components of the reflected light are recorded by the detectors.

Measurements were repeated on both sides of the two samples at two different points on each side.

110 3. Results

Diffuse reflectivity of both bright and matte sides are reported in Figure 4. The first point to note is that measurements repeatability is very good, with some noise for wavelengths higher than 2000 nm. The second point is that bright and matte sides do not have the same diffuse reflectivity. Bright side reflectivity is roughly around 40 %, while matte one is about 75 %. Nevertheless the general trend of the measurements is the same for both sides: 115 the diffuse reflectivity decreases with increasing wavelength with a downhill around 900 nm.

Matte side reflectivities have never been reported in literature. Hence, only bright side results can be compared to measurements made on aluminum deposits or thick rolled aluminum sheets. Furthermore, only few authors reports diffuse reflectivity value. In the case of rolled aluminum, Rönnelid reported a value around 30 %, with the same downward trend as our measurements (23). While, in the case of PVD produced mirrors, diffuse reflectivity 120 can be very low, from less than 10 % down to barely measurable (21).

Figure 6 reports total reflectivity measurements. Once again the repeatability is very good. The trends are the same for both sides. A first plateau in the visible spectrum (around 86 % for the bright side, and 88 % for the matte one), then a downhill around 900 nm bouncing back to values higher than 95 %, followed by a somewhat upward linear trend after 1200 nm. All in all, bright and matte sides of an household aluminum foil have the same 125 total reflectivity spectra. The matte one being, by a small amount - about 2 % -, more reflective than its bright counterpart.

Several total reflectivity spectra, or integrated values, have been reported in literature. Investigations dealing with rolled aluminum report value around between 76.6 and 93.3 % in the visible range (29)(30)(33), and values higher than 90 % in the infrared region (13)(22)(23). Furthermore, their spectra exhibit the same trends as ours 130 (23)(13)(22). For PVD deposited aluminum, the results are mixed. Rincon-Llorente reported results similar to those obtained with rolled sheets, both values and trends (21), while Adelkhani obtained a flat reflectivity spectrum with values higher than 92 % between 300 and 1500 nm (14). The discrepancies may arise from the different polishing / rectification techniques used during the latest stages of the mirrors production.

Using diffuse and total reflectivity measurements, it is possible to compute the specular component of the 135 reflection. It is presented in Figure 7. Both bright and matte side reflectivities increase almost linearly through the measurement range. Bright side specular reflectivity being much higher than its matte counterpart.

Measured values for the bright side are in agreement with other authors findings on rolled aluminum. This is not surprising, as it is a direct consequence of the agreement of diffuse and total reflectivities. A difference can be noted, once again, with PVD produced mirrors. Those mirrors have been reported to have a specular reflectivity 140 higher than 90 % (15)(30). Again, it is tied to the almost zero diffuse component of their reflection. Going one step further, through theoretical development, Xiao He has explained the increasing trend of the specular reflectivity with wavelength (34). Our findings are in agreement with his considerations.

In order to provide readily usable values, several integrals of the reflectivities are available in Table 1. One should

keep in mind that these values are rough estimates as they do not take into account the light source spectrum. The flat profiles of the total reflectivities may make the proposed value of help, the others should be used with caution.

In the view of literature dealing with the reflectivity of aluminum, the angular distribution of the reflected rays has to be discussed. This point has not been dealt with in our work, luckily, other authors have provided valuable insight on this matter. While anodized aluminum has been shown to have a Gaussian isotropic diffuse scattering comprised between $\pm 5^\circ$ (22), the stripes left by the twin roll mills tend to orient reflected light (23)(29). Regardless of the orientation of the incident light - perpendicular or parallel to the stripes - diffuse reflected radiation is distributed on a Gaussian curve (23). This distribution being sharper in the case of the parallel orientation ($\pm 8^\circ$) than in the case of the perpendicular one ($\pm 16^\circ$).

Furthermore, the dependence of reflectivity on the incidence angle has also been addressed. Authors agree on the fact that the total reflectivity does vary much with incident angles between 0 and 78° (23)(35), while diffuse component increases to some extent. Yet results on this topic remain scarce.

4. Application to the lab scale light concentrator

The foreseen design is pictured in Figure 8 (top). The LEDs panel would be placed at one end of a rectangular shaped concentrator, while the photobioreactor would be at the other end, 9 cm away from the outlet. Due to geometrical constraints, the concentrator could be 70 cm long while 22.5 cm high and 13 cm wide at maximum. We chose to work with the maximal dimensions. Indeed the longer the concentrator, the higher the reflected amount of LEDs emitted light. Furthermore, a wide cross sectional area would increase the chance to have a large enough uniform area at the center of the lighted zone into which the photobioreactor is to be placed.

The inner faces of the concentrator are to be coated with aluminum foil, inducing the question of which side of the foil would be best suited. To deal with this question using our measurements, we downloaded Soltrace open source raytracing software, developed by the NREL (32). Soltrace is a C++ coded tool combining a raytracing core and a GUI. It is originally intended to help designing concentrated solar power systems. As it is open source, we have been able to modify it so that a LEDs panel could be modeled as light source, taking into account LEDs number and positions, as well as emitted light angular distribution (from product datasheet OSRAM GW JDSRS1.EC). Soltrace also offers the possibility to take into account reflectivity dependence on incidence angle as well as slope error and diffuse reflection. The latter is modelled as Gaussian distributed (36) which is particularly well-suited in the case of aluminum foil. Figure 9 pictured how reflection is computed taking into account the diffuse component. When reflected, the new direction of the ray is randomly drawn from the Gaussian distribution centered around the specular direction, the key parameter being the variance of distribution.

Finally, benchmarks have shown that its computing capabilities allow it to compete even with commercial codes (37).

5. In silico analysis

The foreseen setup was reproduced into our modified version of Soltrace. A 3D view of the setup and some computed rays is proposed in Figure 8 (bottom). The yellow dotted part is the LEDs panel, the gray rectangles are the concentrator side and the green rectangle is the area into which the photobioreactor has to be positioned. This configuration has been simulated using alternatively bright and matte side of the aluminum foil as internal coating of the concentrator. For each side of the foil, the measurements obtained from the integrating sphere were implemented into Soltrace. Given the fact that photosynthesis is only triggered by 400 to 800 nm radiation, the spectra were integrated over this range only before being incorporated into the code. Those values were used to derive the variance of the Gaussian distribution describing the reflection. To do so, an optimization procedure was used to determine a value that would only leave the specular component of the reflection to escape from our integrating sphere (diameter 110 mm, opening angle 0.004 sr, Sec. 2.2). Finally, reflectivity dependence on incidence angle was not taken into account, as we had no data that could be used to describe it.

In order to compute the lighting over the photobioreactor available area, rays were emitted from the LEDs panel and traced until they reached the targeted zone or escaped the numerical scene. Soltrace uses a Monte Carlo method, i.e. a stochastic approach, meaning that for every hit a random value is drawn (between 0 and 1). If this value is higher than the reflectivity, the ray is absorbed, and the tracing stops, otherwise the ray is reflected and the tracing carries on. The same random procedure is used to determine initial ray direction, yet in this case the random draw is taken out of the light source angular distribution. As a result a large number of rays have to be traced in order to achieve results convergence. Here, 352 millions hits on the targeted area were required to achieve light map convergence in both configurations.

Relative incident light intensities are plotted in Figure 10. This type of plot allows to visualize spatial uniformity of the incident light field. Here, in both cases, an uniform area exists at the center of the foreseen position. This zone is large enough to host our photobioreactor so that it would not be subjected to a core to edge difference higher than 10 % of the averaged incident light intensity.

Hence, another criterion was needed to decide which side of the aluminum foil should be used. Here, the absolute amount of power delivered by the lighting system on the photobioreactor surface was chosen. The bright side delivers 2 % more power than the matte side. Indeed, despite its higher one hit reflectivity, the use of the matte side induces a higher total number of reflection because of its propensity to diffuse scattering. Thus the matte side delivers a lower power onto the photobioreactor.

As a results of this work, we used the bright side of the aluminum foil to build the concentrator. Once finished, in order to validate the predicted incident light map, we used a biology oriented photometer (LICOR LI-250A) to acquire the incident light map on the available area. These measurements and the reproduced map are available in Figure 10 (c). From a qualitative point of view, one can see that the light field predicted by our modified version of Soltrace, fed with our spectra, is in very good agreement with the measurements. From a quantitative point

210 of view, our light concentrator delivers an average light density of $512 \pm 25 \mu\text{molPhoton}/\text{m}^2/\text{s}$ over the culture
volume. The variation is dimmed to be sufficiently low to allow to consider the lighting as uniform. Furthermore,
the maximal intensity is high enough to induce, if desired, light stress.

6. Conclusion

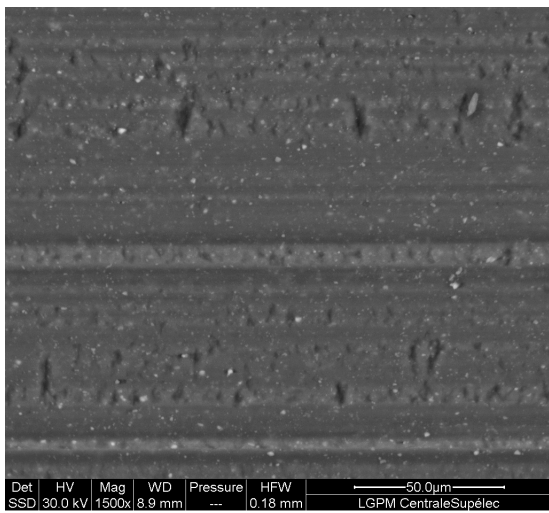
215 This work reports measurements of household aluminum foil reflectivity spectra on both bright and matte
sides. These measurements were done using an integrating sphere, over a 250 - 2500 nm range. Diffuse and total
reflectivities were acquired, for two samples each time. The obtained results are very repeatable and in good
agreement with literature on rolled aluminum sheets, for the bright side at least, as matte side data were not found.

This work revealed that, behind the closeness of the total reflectivities of both sides, an important difference
exists. Specular reflectivity is higher for the bright side while diffuse reflectivity is higher for the matte one. Our
220 measurements are readability usable and available as supplementary materials.

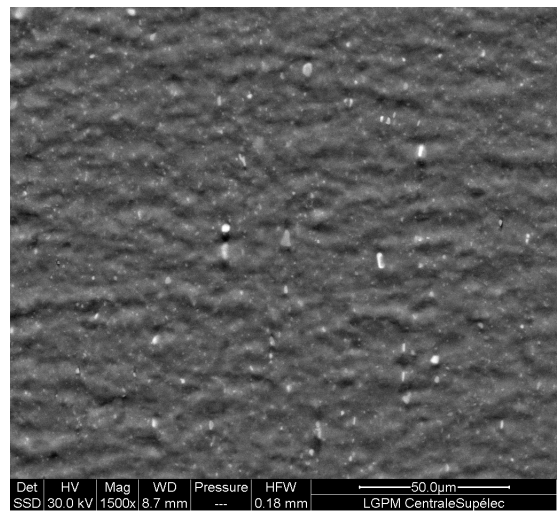
Finally, we applied these findings to the in silico design of lab scale light concentrator illuminating a new
photobioreactor. A modified version of the raytracing software Soltrace was used to determine which of the two
sides of our household aluminum foil was best suited for our application. Interestingly, even though bright side
has the lowest total reflectivity, it turned out to be better suited than the matte one. The explanation lies in the
225 number of additional reflections induced by the matte side higher diffuse reflectivity.

	Matte side (%)			Bright side (%)		
	Specular	Diffuse	Total	Specular	Diffuse	Total
Visible: 390 – 700 nm	9.7	77.9	87.6	38.4	47.9	86.3
PAR: 400 – 800 nm	10.2	76.9	87.1	39.3	46.7	86.0
NIR: 750 – 2500 nm	23.0	75.4	98.4	57.0	39.3	96.2
Whole range: 250 – 2500 nm	19.8	76.2	96.1	52.5	41.5	94.0

Table 1: Averaged reflectivities over different spectral ranges. PAR: Photosynthetically Active Radiation, NIR: Near InfraRed



(a)



(b)

Figure 1: SEM observation, magnification x1600. (a) bright side, (b) matte side

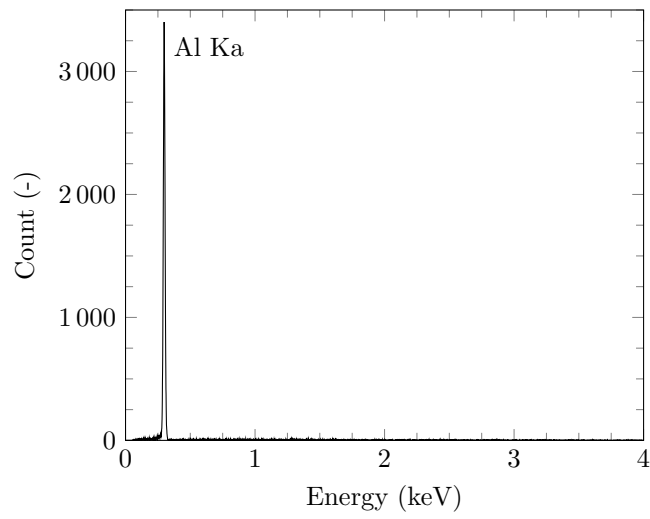


Figure 2: Bright side energy-dispersive X-ray spectroscopy spectrum: Al 93.84 %, O 4.14 %, Ca 1.20 %, Fe 0.82 %

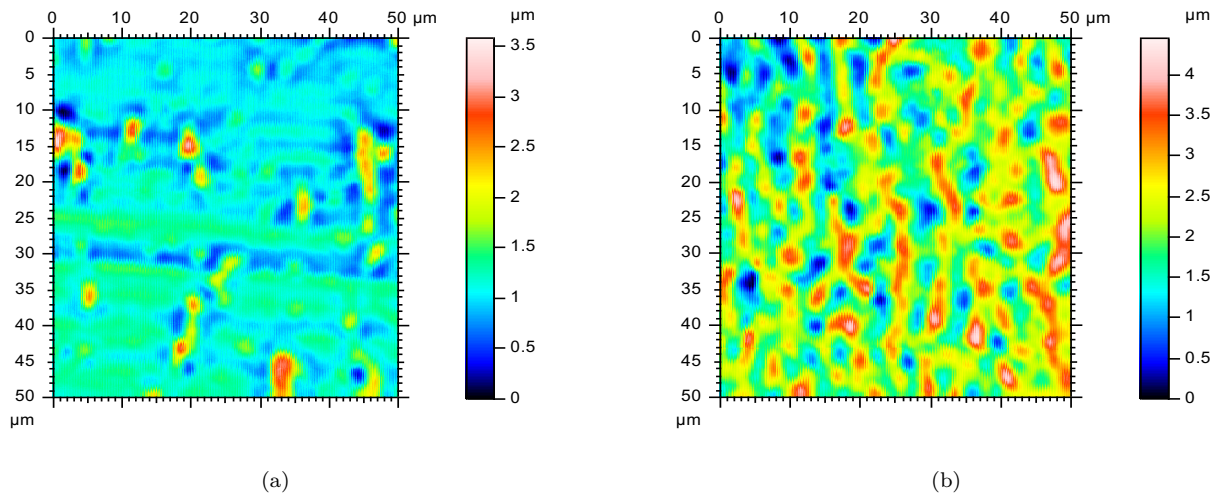


Figure 3: Roughness map (x, y resolution 0.2 μm , z precision 10 nm). (a) bright side, (b) matte side

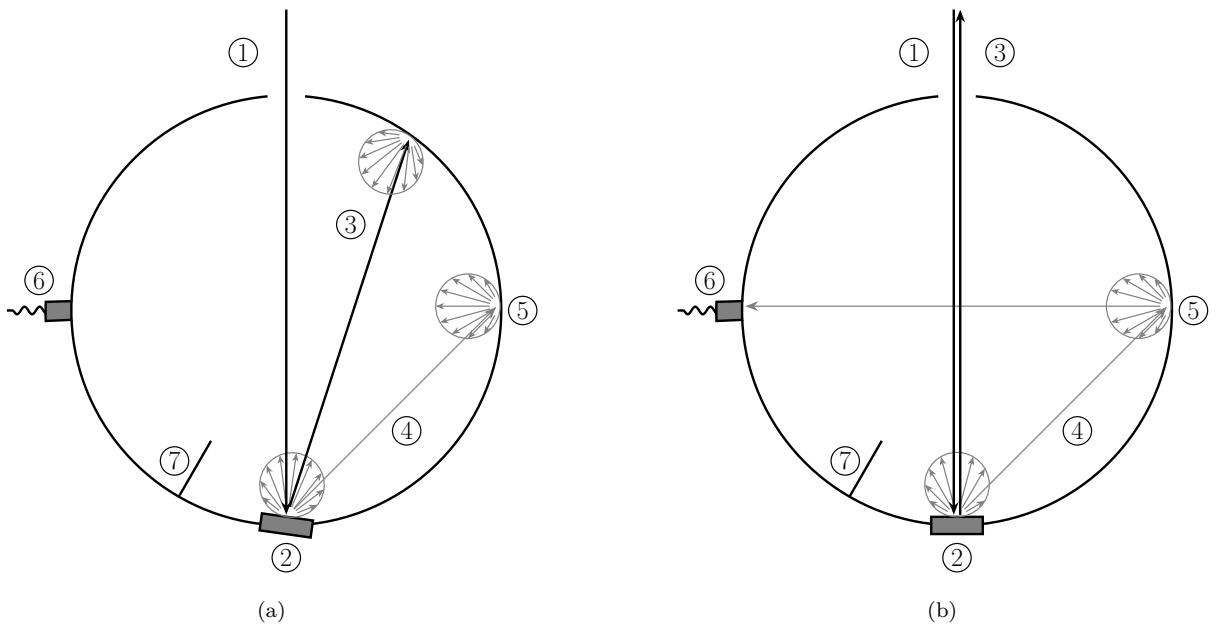


Figure 4: Integrating sphere working principle. (a) diffuse reflectivity measurement, sample tilted at $3^{\circ}20'$ (b) total reflectivity measurement. (1) incident ray, (2) sample, (3) specular reflected ray, (4) diffuse reflected ray, (5) reflection of the diffuse radiation, (6) detector, (7) baffle to prevent first reflection direct hit on the detector

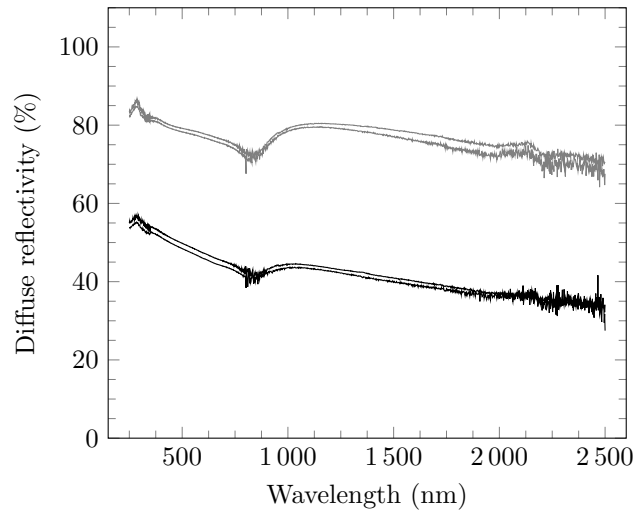


Figure 5: Aluminum foil diffuse reflectivity, at two different points on each side. Black: bright side, gray: matte side

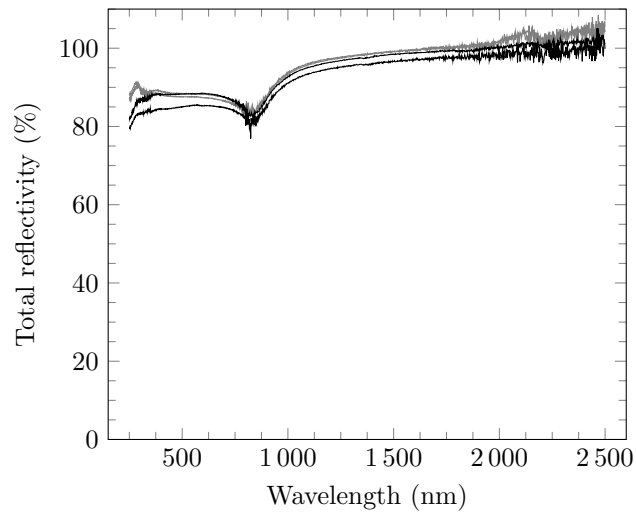


Figure 6: Aluminum foil total reflectivity, at two different points on each side. Black: bright side, gray: matte side

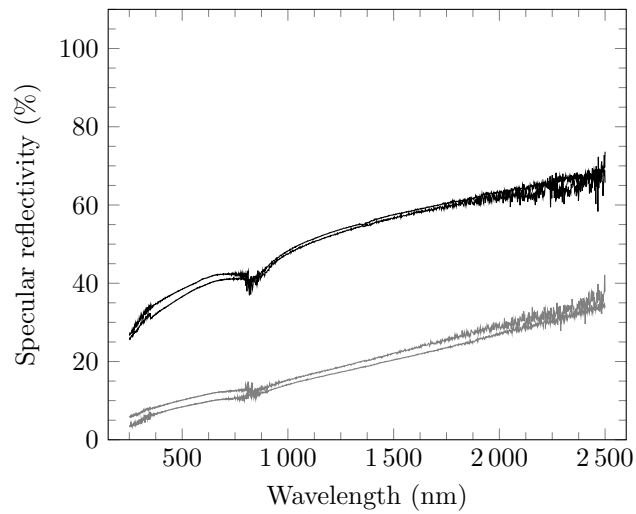


Figure 7: Aluminum foil specular reflectivity, at two different points on each side. Black: bright side, gray: matte side

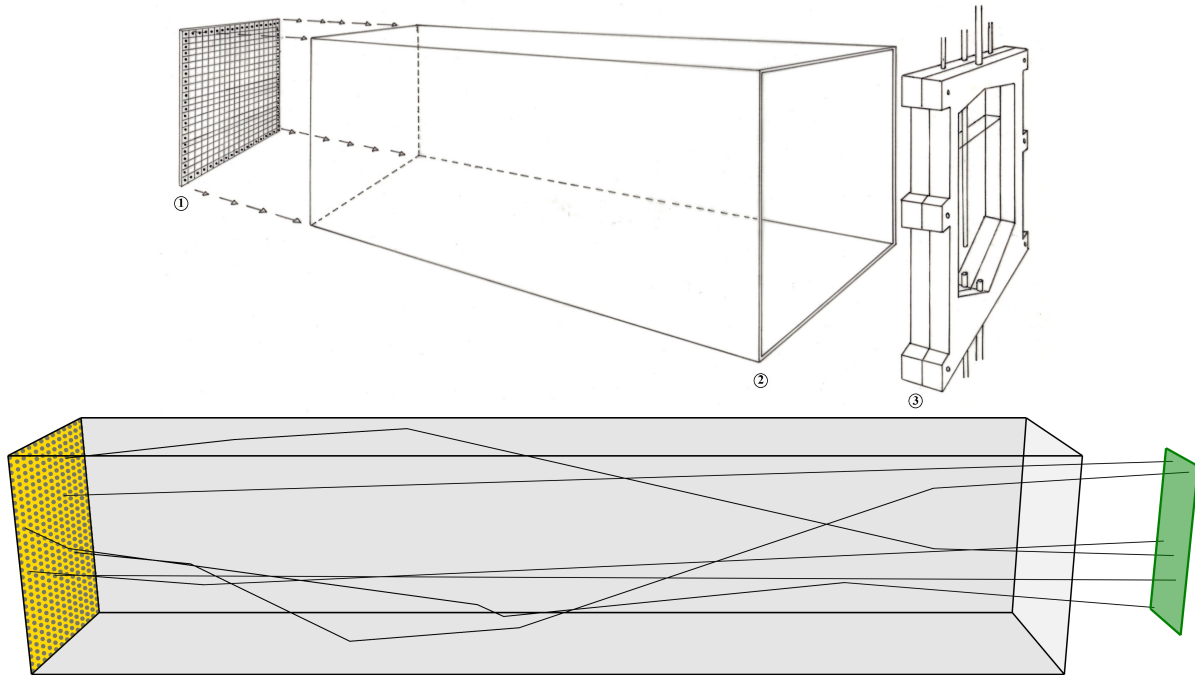


Figure 8: Top - Scheme of the photobioreactor and its lighting system. (1) LEDs panel; (2) aluminum coated concentrator; (3) flat panel photobioreactor. Bottom - Numerical scene with some traced rays. Yellow: LEDs panel, gray: aluminum reflectors (bright side), green: rectangle into which the photobioreactor has to be positioned

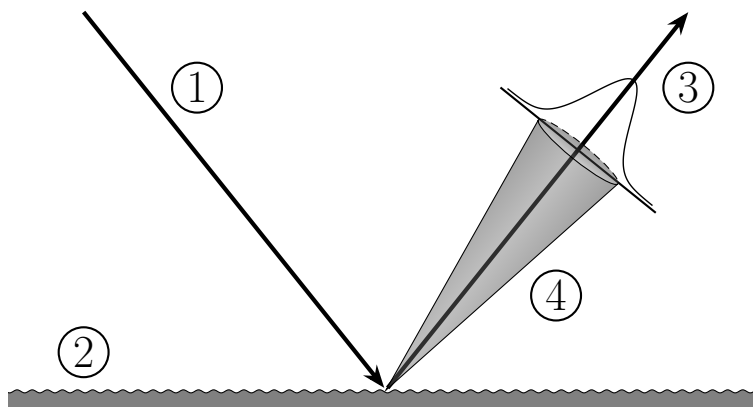


Figure 9: Soltrace raytracing procedure illustration. (1) incident ray, (2) foil surface, with roughness inducing diffuse reflection (3) specular reflection direction, (4) Gaussian distribution used to model reflection (spread overestimated for illustrating purposes)

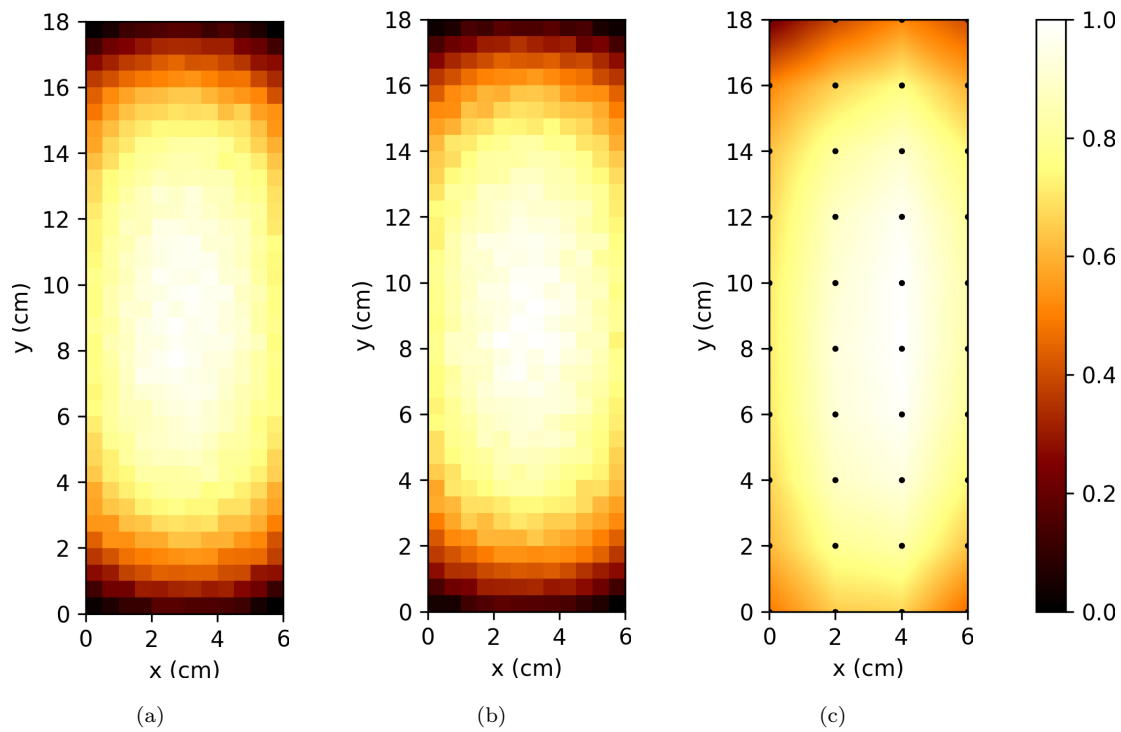


Figure 10: (a & b) Predicted relative intensity map over the area available to position the photobioreactor. (a) light reflected by the bright side. (b) light reflected by the matte side. Map resolution: 5 mm x 5 mm, 352 millions rays for each. (c) Measured relative intensity map over the reactor, light reflected by the bright side. Black dot: measurement positions. Colormap reconstituted via Delaunay triangulation

References

- [1] L. Straka, B. E. Rittmann, Dynamic response of *synechocystis* sp. pcc 6803 to changes in light intensity, *Algal research* 32 (2018) 210–220.
- [2] A. M. Kliphuis, L. de Winter, C. Vejrazka, D. E. Martens, M. Janssen, R. H. Wijffels, Photosynthetic efficiency of *chlorella sorokiniana* in a turbulently mixed short light-path photobioreactor, *Biotechnology progress* 26 (3) (2010) 687–696.
- [3] H. Qiang, A. Richmond, Productivity and photosynthetic efficiency of *spirulina platensis* as affected by light intensity, algal density and rate of mixing in a flat plate photobioreactor, *Journal of Applied Phycology* 8 (2) (1996) 139–145.
- [4] J. B. Schou, D. L. Jeffers, J. G. Streeter, Effects of Reflectors, Black Boards, or Shades Applied at Different Stages of Plant Development on Yield of Soybeans 1, *Crop Science* 18 (1) (1978) 29–34. doi:10.2135/cropsci1978.0011183X001800010009x. URL <https://dl.sciencesocieties.org/publications/cs/abstracts/18/1/CS0180010029>
- [5] S. C. Kehoe, T. M. Joyce, P. Ibrahim, J. B. Gillespie, R. A. Shahar, K. G. McGuigan, Effect of agitation, turbidity, aluminium foil reflectors and container volume on the inactivation efficiency of batch-process solar disinfectors (Mar. 2001). doi:10.1016/S0043-1354(00)00353-5. URL <http://www.sciencedirect.com/science/article/pii/S0043135400003535>
- [6] H. Tabaei, M. Ameri, The Effect of Booster Reflectors on the Photovoltaic Water Pumping System Performance, *Journal of Solar Energy Engineering* 134 (1) (2011) 014501–014501–4. doi:10.1115/1.4005339. URL <http://dx.doi.org/10.1115/1.4005339>
- [7] K. R. Narahari, S. Mishra, V. Hegde, K. A. Kumar, C. Prabhu, N. Chaulagain, Enhanced radiation trapping technique using low-cost aluminium flat plate reflector a performance analysis on solar PV modules, in: 2017 2nd International Conference for Convergence in Technology (I2CT), 2017, pp. 416–420. doi:10.1109/I2CT.2017.8226163.
- [8] A. Yadav, M. Kumar, Experimental Study and Analysis of Parabolic trough Collector with Various Reflectors, *International Journal of Energy and Power Engineering* 7 (12) (2013) 5.
- [9] Y. Zhao, H. Zheng, B. Sun, C. Li, Y. Wu, Development and performance studies of a novel portable solar cooker using a curved Fresnel lens concentrator, *Solar Energy* 174 (2018) 263–272. doi:10.1016/j.solener.2018.09.007. URL <http://www.sciencedirect.com/science/article/pii/S0038092X18308788>
- [10] J. Llorente, J. Ballestrín, A. J. Vázquez, A new solar concentrating system: Description, characterization and applications, *Solar Energy* 85 (5) (2011) 1000–1006. doi:10.1016/j.solener.2011.02.018. URL <http://www.sciencedirect.com/science/article/pii/S0038092X11000624>
- [11] O. Keles, M. Dundar, Aluminum foil: Its typical quality problems and their causes, *Journal of Materials Processing Technology* 186 (1) (2007) 125–137. doi:10.1016/j.jmatprotec.2006.12.027. URL <http://www.sciencedirect.com/science/article/pii/S0924013606011678>
- [12] Aluminium foil, page Version ID: 876160613 (Dec. 2018). URL https://en.wikipedia.org/w/index.php?title=Aluminium_foil&oldid=876160613
- [13] J. Bartl, M. Baranek, Emissivity of aluminium and its importance for radiometric measurement, *MEASUREMENT SCIENCE REVIEW* 4 (2004) 6.
- [14] H. Adelkhani, S. Nasoodi, A. H. Jafari, A study of the Morphology and Optical Properties of Electropolished Aluminum in the Vis-IR region, *Int. J. Electrochem. Sci.* 4 (2009) 9.
- [15] J. Campos, J. Fontecha, A. Pons, P. Corredera, A. Corróns, Measurement of standard aluminium mirrors, reflectance versus light polarization, *Measurement Science and Technology* 9 (2) (1998) 256. doi:10.1088/0957-0233/9/2/013. URL <http://stacks.iop.org/0957-0233/9/i=2/a=013>
- [16] J. Harrison, Investigation of Reflective Materials for the Solar Cooker, Tech. rep., Florida Solar Energy Center (2001).

- [17] T. Babeva, S. Kitova, B. Mednikarov, I. Konstantinov, Preparation and characterization of a reference aluminium mirror, *Applied Optics* 41 (19) (2002) 3840–3846. doi:10.1364/AO.41.003840.
275 URL <https://www.osapublishing.org/ao/abstract.cfm?uri=ao-41-19-3840>
- [18] M. F. Crawford, W. M. Gray, A. L. Schawlow, F. M. Kelly, Transmission and Reflection Coefficients of Aluminium Films for Interferometry, *JOSA* 39 (10) (1949) 888–888. doi:10.1364/JOSA.39.000888.
URL <https://www.osapublishing.org/josa/abstract.cfm?uri=josa-39-10-888>
- [19] C. M. Ankenbrandt, E. M. Lent, Increasing the Light Collection Efficiency of Scintillation Counters, *Review of Scientific Instruments* 34 (6) (1963) 647–651. doi:10.1063/1.1718530.
280 URL <https://aip.scitation.org/doi/abs/10.1063/1.1718530>
- [20] J. De Laet, H. Terryn, J. Vereecken, The use of impedance spectroscopy and optical reflection spectroscopy to study modified aluminium surfaces, *Electrochimica Acta* 41 (7) (1996) 1155–1161. doi:10.1016/0013-4686(95)00466-1.
285 URL <http://www.sciencedirect.com/science/article/pii/S0013468695004661>
- [21] G. Rincón-Llorente, I. Heras, E. Guillén Rodríguez, E. Schumann, M. Krause, R. Escobar-Galindo, On the Effect of Thin Film Growth Mechanisms on the Specular Reflectance of Aluminium Thin Films Deposited via Filtered Cathodic Vacuum Arc, *Coatings* 8 (9) (2018) 321. doi:10.3390/coatings8090321.
URL <https://www.mdpi.com/2079-6412/8/9/321>
- [22] M. Brogren, A. Helgesson, B. Karlsson, J. Nilsson, A. Roos, Optical properties, durability, and system aspects of a new aluminium-polymer-laminated steel reflector for solar concentrators, *Solar Energy Materials and Solar Cells* 82 (3) (2004) 387–412. doi:10.1016/j.solmat.2004.01.029.
290 URL <http://www.sciencedirect.com/science/article/pii/S0927024804000522>
- [23] M. Rönnelid, M. Adsten, T. Lindström, P. Nostell, E. Wäckelgård, Optical scattering from rough-rolled aluminium surfaces, *Applied Optics* 40 (13) (2001) 2148–2158. doi:10.1364/AO.40.002148.
295 URL <https://www.osapublishing.org/ao/abstract.cfm?uri=ao-40-13-2148>
- [24] P. Feliński, R. Sekret, Effect of a low cost parabolic reflector on the charging efficiency of an evacuated tube collector/storage system with a PCM, *Solar Energy* 144 (2017) 758–766. doi:10.1016/j.solener.2017.01.073.
URL <http://www.sciencedirect.com/science/article/pii/S0038092X17300828>
- [25] J. Wang, P. Andrews, C. Butler, E. McAlpine, G. Scamans, X. Zhou, Optical cleanliness measurement methods for aluminium sheet surfaces, *Surface and Interface Analysis* 0 (0). doi:10.1002/sia.6566.
300 URL <https://www.onlinelibrary.wiley.com/doi/abs/10.1002/sia.6566>
- [26] J. I. Ajona, A. Vidal, The use of CPC collectors for detoxification of contaminated water: Design, construction and preliminary results, *Solar Energy* 68 (1) (2000) 109–120. doi:10.1016/S0038-092X(99)00047-X.
305 URL <http://www.sciencedirect.com/science/article/pii/S0038092X9900047X>
- [27] J. Franco, L. Saravia, V. Javi, R. Caso, C. Fernandez, Pasteurization of goat milk using a low cost solar concentrator, *Solar Energy* 82 (11) (2008) 1088–1094. doi:10.1016/j.solener.2007.10.011.
URL <http://www.sciencedirect.com/science/article/pii/S0038092X07002253>
- [28] M. Fairlie, J. G. Akkerman, R. S. Timsit, Optical Techniques For The Surface Evaluation Of Bright Aluminum Sheet, in: *Optical Techniques for Industrial Inspection*, Vol. 0665, International Society for Optics and Photonics, 1986, pp. 32–39. doi:10.1117/12.938724.
310 URL <https://www.spiedigitallibrary.org/conference-proceedings-of-spie/0665/0000/Optical-Techniques-For-The-Surface-Evaluation-Of-Bright-Aluminum-Sheet/10.1117/12.938724.short>
- [29] I. Lindseth, A. Bardal, R. Spooren, Reflectance measurements of aluminium surfaces using integrating spheres, *Optics and Lasers in Engineering* 32 (5) (1999) 419–435. doi:10.1016/S0143-8166(00)00010-5.
315 URL <http://www.sciencedirect.com/science/article/pii/S0143816600000105>
- [30] L. Holland, B. J. Williams, The effect of aluminium purity on the reflectivity of evaporated front surface mirrors, *Journal of Scientific Instruments* 32 (7) (1955) 287. doi:10.1088/0950-7671/32/7/119.
320 URL <http://stacks.iop.org/0950-7671/32/i=7/a=119>

- [31] J. Thirlwell, Characteristic energy losses of low-energy electrons reflected from aluminium and copper, *Journal of Physics C: Solid State Physics* 1 (4) (1968) 979. doi:10.1088/0022-3719/1/4/318.
URL <http://stacks.iop.org/0022-3719/1/i=4/a=318>
- 325 [32] T. Wendelin, Soltrace: a new optical modeling tool for concentrating solar optics, in: *ASME 2003 International Solar Energy Conference*, American Society of Mechanical Engineers, 2003, pp. 253–260.
- [33] A. Seifter, K. Boboridis, A. W. Obst, Emissivity Measurements on Metallic Surfaces with Various Degrees of Roughness: A Comparison of Laser Polarimetry and Integrating Sphere Reflectometry (Mar. 2004). doi:10.1023/B:IJOT.0000028489.81327.b7.
URL <https://doi.org/10.1023/B:IJOT.0000028489.81327.b7>
- 330 [34] X. D. He, K. E. Torrance, F. X. Sillion, D. P. Greenberg, A Comprehensive Physical Model for Light Reflection, in: *Proceedings of the 18th Annual Conference on Computer Graphics and Interactive Techniques, SIGGRAPH '91*, ACM, New York, NY, USA, 1991, pp. 175–186. doi:10.1145/122718.122738.
URL <http://doi.acm.org/10.1145/122718.122738>
- 335 [35] M. Janecek, W. W. Moses, Optical Reflectance Measurements for Commonly Used Reflectors, *IEEE Transactions on Nuclear Science* 55 (4) (2008) 2432–2437. doi:10.1109/TNS.2008.2001408.
- [36] T. Wendelin, A. Dobos, A. Lewandowski, Soltrace: a ray-tracing code for complex solar optical systems, *Contract 303* (2013) 275–3000.
- 340 [37] J. Yellowhair, J. M. Christian, C. K. Ho, Evaluation of solar optical modeling tools for modeling complex receiver geometries, in: *ASME 2014 8th International Conference on Energy Sustainability collocated with the ASME 2014 12th International Conference on Fuel Cell Science, Engineering and Technology*, American Society of Mechanical Engineers, 2014, pp. V001T02A048–V001T02A048.